

Regge Trajectories with Square-Root Branch Points and Their Regge Cuts*

J. B. Bronzan

Department of Physics, Rutgers University, New Brunswick, New Jersey 08903

M. L. Goldberger

Joseph Henry Laboratories, Princeton University, Princeton, New Jersey 08540

(Received 15 June 1973)

We discuss branch points in the complex angular momentum plane formed by two Regge poles on trajectories with square-root branch points at $t = 0$. We find several new cuts which collide with the expected Mandelstam cuts at $t = 0$. In the bootstrap of the Pomeranchon pole, the collection of cuts has the same effect as in the case of linear trajectories: The Pomeranchon can have $\alpha(0) = 1$ only if certain couplings vanish at $t = 0$.

I. INTRODUCTION

The structure of partial-wave scattering amplitudes extended into the complex angular momentum plane (j plane) has been of interest for over a decade. In simple models it is known that the amplitude has Regge poles of the form $\beta(t) \times [j - \alpha(t)]^{-1}$ with the trajectory function $\alpha(t)$ analytic in the t plane except for branch points at positive t values corresponding to physical thresholds in that channel.¹ There may be singularities in the trajectories (branch points) at values of $t \leq 0$ if several trajectories coincide. Finally, there are known to be branch points in the amplitude, $f(t, j)$, that arise when two or more Regge poles are exchanged by the scattering particles, or, stated otherwise, when certain multiparticle processes are taken into account.

In this paper we discuss what happens to the structure of the scattering amplitude when two Regge poles combine to lead to branch points in the j plane, and the Regge-pole trajectories themselves have branch points in the t plane at $t = 0$. In particular, we shall study trajectories of the form $\alpha_{\pm}(t) = \alpha \pm i A\sqrt{-t} + \gamma t$, called Schwarz trajectories.² There are several motivations for looking into this question. Such trajectories with $\alpha = 1$ appear in the Regge-eikonal model,³ in models of the violation of the Pomeranchuk theorem,^{4,5} in certain bootstrap models of the Pomeranchon,⁶

and in models of diffraction scattering in which the diffraction pattern shrinks faster than $(\ln s)^{-1}$.⁵ In connection with the bootstrap of the Pomeranchon pole, the Pomeranchon cannot have $\alpha(0) = 1$ if $\alpha'(0)$ is finite and certain Regge couplings are nonzero, and it is interesting to see if these arguments are modified by the Pomeranchon's association with Schwarz trajectories. In addition, one of the authors has given a discussion of the branch points based on continuing l -channel unitarity relations from $t > 16 m_{\pi}^2$ to $t \leq 0$.⁷ This approach leads to predictions about the nature of the two-Reggeon cuts located at $\alpha_{c_{\pm}}(t) = 2\alpha_{\pm}(\frac{1}{2}t) - 1$. However, we shall see that there are other, unexpected cuts in the angular momentum plane which are discovered only when one formulates the dynamics in the scattering region from the start. For this reason, the present paper constitutes a correction to Ref. 7.

The first step in our study is to set up the dynamics, and for the reasons stated above we want the formulation to be at $t \leq 0$, with no continuation required. To this end, we have studied the structure of the partial-wave amplitude in both the multiperipheral model and Gribov's Reggeon calculus. We present our results in Appendixes A and B. These quite different formulations agree that the analytic structure is given by the two-Reggeon-cut integral

$$f(t, j) = f_{++} + f_{+-} + f_{-+} + f_{--},$$

$$f_{ij}(t, j) = \frac{1}{\pi} \int_{-t_0}^0 dt_1 \int_{-t_0}^0 dt_2 \frac{\theta(-\Delta(t, t_1, t_2))}{[-\Delta(t, t_1, t_2)]^{1/2} [j+1 - \alpha_i(t_1) - \alpha_j(t_2)]}, \tag{1.1}$$

where the triangle function $\Delta(a, b, c) = a^2 + b^2 + c^2 - 2ab - 2ac - 2bc$ and t_0 is some (irrelevant) constant. It is not difficult to see, incidentally, that if the α 's are monotonically increasing, the max-

imum value of $\Lambda(t_1, t_2) = \alpha_i(t_1) + \alpha_j(t_2) - 1$ (which determines the rightmost singularity in the j plane) occurs on the boundary of the integration region, $\Delta(t, t_1, t_2) = 0$. This in turn is $\sqrt{-t_1} + \sqrt{-t_2}$

$=\sqrt{-t}$. If the two trajectories are the same, by symmetry the extreme value of Λ is $2\alpha(\frac{1}{4}t) - 1$, the familiar Mandelstam, Amati-Stanghellini-Fubini (ASF) branch point.⁸

It is crucial that the four cut terms be added with equal weights, as in Eq. (1.1). In particular, the $+$, $-$ terms are important, in contrast with common belief and the statement made in Ref. 7. We present two arguments. First, we use the expansion⁹

$$\begin{aligned} & \frac{1}{\pi} \int_{-t_0}^0 dt_1 \int_{-t_0}^0 dt_2 \frac{\theta(-\Delta(t, t_1, t_2))g(t_1, t_2)}{[-\Delta(t, t_1, t_2)]^{1/2}} \\ &= \sum_{n=0}^{\infty} \frac{(-t)^n}{(n!)^2} \int_{-t_0}^0 du u^n \frac{\partial^{2n}}{\partial t_1^n \partial t_2^n} g(t_1, t_2) \Big|_{t_1=t_2=u}. \end{aligned} \quad (1.2)$$

Applying this at $t=0$, we find that f_{ij} are singular at $j=2\alpha-1$, with behaviors

$$\begin{aligned} f_{++}(0, j) &\sim f_{--}(0, j) \\ &\sim -\frac{1}{2A^2} (j+1-2\alpha) \ln(j+1-2\alpha), \\ f_{+-}(0, j) &= f_{-+}(0, j) \\ &\sim -\frac{1}{2\gamma} \ln(j+1-2\alpha). \end{aligned} \quad (1.3)$$

Thus the $+$, $-$ terms are singular and dominant at $t=0$ and $j=2\alpha-1$.

The second argument involves analyticity in the energy variable. For $\text{Re } j > 2\alpha - 1$, the denominators in the f_{ij} may be expressed

$$\begin{aligned} & [j+1-\alpha_i(t_1)-\alpha_j(t_2)]^{-1} \\ &= \int_0^{\infty} dy \exp\{-y[j+1-\alpha_i(t_1)-\alpha_j(t_2)]\}. \end{aligned} \quad (1.4)$$

Inserting this and Eq. (1.2) into Eq. (1.1) we find

$$\begin{aligned} f(t, j) &= \sum_{n=0}^{\infty} \frac{(-t)^n}{(n!)^2} \int_0^{\infty} dy e^{-y(j+1)} \\ &\quad \times \int_{-t_0}^0 du u^n \left[\frac{\partial^n}{\partial u^n} \left(e^{y\alpha_+(u)} + e^{y\alpha_-(u)} \right) \right]^2. \end{aligned} \quad (1.5)$$

The integrand of the u integral in Eq. (1.5) is inte-

grable at $u=0$ because both trajectories are present, and $f(t, j)$ is analytic at $t=0$ for $\text{Re } j > 2\alpha - 1$. On the other hand, the partial sum $f_{++} + f_{--}$ has the last factor in Eq. (1.5) replaced by

$$\left[\frac{\partial^n}{\partial u^n} e^{y\alpha_+(u)} \right]^2 + \left[\frac{\partial^n}{\partial u^n} e^{y\alpha_-(u)} \right]^2, \quad (1.6)$$

which behaves like u^{1-2n} at $u=0$. The second and higher derivatives of $f_{++} + f_{--}$ with respect to t do not exist at $t=0$, and the partial sum has a fixed branch point at $t=0$ for large positive j . From Eq. (1.1) it is evident that $f_{++} + f_{--}$ is real for $t < 0$ and large positive j , so the partial sum must be complex for $t > 0$ and large positive j . This is in disagreement with independently established analyticity properties. Only when one adds the four f_{ij} 's with the same weight is the illegal branch point at $t=0$ removed.

II. GENERAL SINGULARITY ANALYSIS

The integral $f(t, j)$ has many singularities in the j plane in addition to the Mandelstam cuts, and we begin the study of f by listing all possible singularities. We transform to the variables u, ϕ :

$$\begin{aligned} t_1 &= u + \frac{1}{4}t + (ut)^{1/2} \cos \phi, \\ t_2 &= u + \frac{1}{4}t - (ut)^{1/2} \cos \phi. \end{aligned} \quad (2.1)$$

When the four terms are added, the integral over ϕ can be evaluated:

$$\begin{aligned} f &= f_1 + f_2, \\ f_1 &= 2 \int_{-t_0}^0 du \left(\frac{b}{ac} \right)^{1/2}, \\ f_2 &= 2 \int_{-t_0}^0 du \left(\frac{c}{ab} \right)^{1/2}, \\ a &= \beta^2 - 4A^2(u + \frac{1}{4}t), \\ b &= \beta^2 - 4A^2u, \\ c &= \beta^2 - A^2t, \\ \beta &= j + 1 - 2\alpha - 2\gamma u - \frac{1}{2}\gamma t. \end{aligned} \quad (2.2)$$

f_1 and f_2 have six linear factors under the square roots; they are hyperelliptic integrals. These factors can be exhibited:

$$a = 4\gamma^2(u - u_{a+})(u - u_{a-}), \text{ etc.},$$

$$\begin{aligned} u_{a\pm} &= \frac{1}{2\gamma^2} \left\{ \gamma(j+1-2\alpha - \frac{1}{2}\gamma t) + A^2 \pm A [2\gamma(j+1-2\alpha - \frac{1}{2}\gamma t) + \gamma^2 t + A^2]^{1/2} \right\}, \\ u_{b\pm} &= \frac{1}{2\gamma^2} \left\{ \gamma(j+1-2\alpha - \frac{1}{2}\gamma t) + A^2 \pm A [2\gamma(j+1-2\alpha - \frac{1}{2}\gamma t) + A^2]^{1/2} \right\}, \\ u_{c\pm} &= \frac{1}{2\gamma} [j+1-2\alpha - \frac{1}{2}\gamma t \pm iA(-t)^{1/2}]. \end{aligned} \quad (2.3)$$

The possible singularities of f are the following:

(a) *End-point singularities.* These occur when one of $u_{a\pm}$, $u_{b\pm}$, and $u_{c\pm}$ is at $u=0$. (End-point singularities at $u=-t_0$ are spurious, and will be ignored.) Such singularities are easily located by asking when the constant terms in the quadratic forms a , b , and c vanish.

(1) $u_{a\pm}=0$. These singularities satisfy $(j+1-2\alpha-\frac{1}{2}\gamma t)^2-A^2t=0$. These are the Mandelstam cuts, which we denote $\alpha_{c\pm}(t)$.

(2) $u_{b\pm}=0$. The singularity satisfies $(j+1-2\alpha-\frac{1}{2}\gamma t)^2=0$. We designate this as $\alpha_1(t)$:

$$\alpha_1(t)=2\alpha-1+\frac{1}{2}\gamma t. \tag{2.4}$$

$\alpha_1(t)$ coincides with the Mandelstam cut in the linear limit $A=0$.

(3) $u_{c\pm}=0$. We again obtain the Mandelstam cuts $\alpha_{c\pm}(t)$.

(b) *Pinch singularities.* These can occur when $u_{a+}=u_{a-}$, $u_{b+}=u_{b-}$, or $u_{c+}=u_{c-}$. The location of these singularities can be read off from Eq. (2.3).

(1) $u_{a+}=u_{a-}$. The singularity is a fixed cut at j_0 ,

$$j_0=2\alpha-1-\frac{A^2}{2\gamma}. \tag{2.5}$$

(2) $u_{b+}=u_{b-}$. The singularity occurs at

$$\alpha_2(t)=2\alpha-1-\frac{A^2}{2\gamma}+\frac{1}{2}\gamma t. \tag{2.6}$$

This, too, coincides with the Mandelstam cut in the linear limit.

(3) $u_{c+}=u_{c-}$. The singularity is at $t=0$. Further pinches occur when two of the forms a , b , and c vanish at the same value of u . The locations of singularities generated in this way can be read off from Eqs. (2.2).

(4) $a=b=0$. Then $t=0$.

(5) $a=c=0$. Then $u=0$ and $j=\alpha_{c\pm}(t)$.

(6) $b=c=0$. Then $t=4\mu$, and the singularities satisfy $(j+1-2\alpha-\gamma t)^2-A^2t=0$. These singularities coincide with the input pole trajectories $j=\alpha_{\pm}(t)$.

In summary, possible singularities occur at $j=\alpha_{c\pm}(t)$, $\alpha_{\pm}(t)$, $\alpha_1(t)$, $\alpha_2(t)$, j_0 , and at $t=0$. There are no non-Landau singularities because $u_{a\pm}$, $u_{b\pm}$, and $u_{c\pm}$ are finite for finite j and t .

III. PHYSICAL-SHEET SINGULARITIES FOR $t \leq 0$

We next determine which of the singularities obtained in Sec. II are on the physical sheet of f for $t < 0$, and obtain the threshold behavior of f at singularities. It is clear from Eq. (1.1) that for j large and real, f is real. We can examine the points α_1 , α_2 , and j_0 , which are real, by re-

ducing j from large positive values along the real j axis. As we do this, we must watch whether the singularities of the integrands of f_1 and f_2 approach the negative u axis and deform the integration contour. Clearly the branch points $u_{c\pm}$, which are complex, cannot approach or deform the integration contour. The motions of other singularities of the integrands are illustrated in Fig. 1. The only singularity that reaches $u=0$ is u_{b-} at $j=\alpha_1(t)$. However, because this curve is tangent to $u=0$, the integration contours are only deformed for $j < \alpha_1(t)$, and neither f_1 nor f_2 is singular at $\alpha_1(t)$. The deformations of the integration contours in Eq. (2.2) are illustrated in Fig. 2. For either continuation around $j=\alpha_1(t)$, f_1 and f_2 acquire the same anomalous extension:

$$\begin{aligned} f_1 &= 2 \int_{-t_0}^0 du \left[\frac{b}{ac} \right]^{1/2} + 4 \int_0^{u_{b-}} du \left[\frac{b}{ac} \right]^{1/2}, \\ f_2 &= 2 \int_{-t_0}^0 du \left[\frac{c}{ab} \right]^{1/2} + 4 \int_0^{u_{b-}} du \left[\frac{c}{ab} \right]^{1/2}. \end{aligned} \tag{3.1}$$

The anomalous branch point collides with u_{b+} at $j=\alpha_2(t)$, producing a singularity of f . The discontinuities across this cut in the j plane are

$$\begin{aligned} \Delta_j f_1(t, j) &= \frac{1}{2i} [f_1(t, j+i\epsilon) - f_1(t, j-i\epsilon)] \\ &= -\frac{2}{i} \int_{u_{b-}}^{u_{b+}} du \left[\frac{b}{ac} \right]^{1/2}, \\ \Delta_j f_2(t, j) &= -\frac{2}{i} \int_{u_{b-}}^{u_{b+}} du \left[\frac{c}{ab} \right]^{1/2}, \quad j < \alpha_2(t). \end{aligned} \tag{3.2}$$

For $j < \alpha_2(t)$, u_{b+} and u_{b-} are complex conjugates. The integrals in Eq. (3.2) run along the line

$$\text{Re } u = \frac{1}{2\gamma} (j+1-2\gamma-\frac{1}{2}\gamma t) + \frac{A^2}{2\gamma^2}.$$

At $\text{Im } u=0$, the integrands are real and positive. The discontinuities in Eq. (3.2) are themselves hyperelliptic integrals, but for j close enough to $\alpha_2(t)$ only the variation of the factor b is significant. In this limit f_2 dominates, and f has a log-

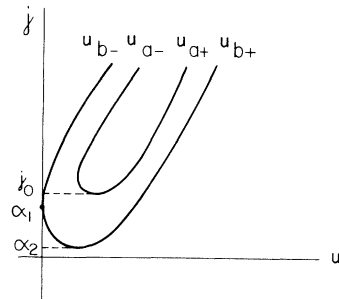


FIG. 1. Motion of singularities of integrands of f_1 and f_2 as j is varied. Only the real branches are shown.

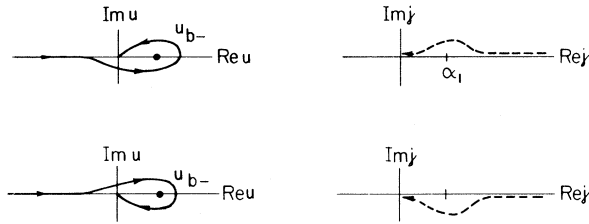


FIG. 2. Integration contours of f_1 and f_2 when j is continued below α_1 as shown.

arithmetic singularity at $\alpha_2(t)$. Near $j = \alpha_2(t)$

$$f(t, j) \sim -\frac{1}{\gamma} \left[\frac{A^2 - \gamma^2 t}{-\gamma^2 t} \right]^{1/2} \ln[j - \alpha_2(t)]. \quad (3.3)$$

As $t \rightarrow 0$, the neighborhood around $j = \alpha_2(t)$ in which Eq. (3.3) is adequate shrinks to zero.

The possible singularities $\alpha_{c+}(t)$ and $\alpha_+(t)$ can be examined by setting $j = iA\sqrt{-t} + \xi$, where ξ is real, and then reducing ξ from large positive values. During this continuation, none of the singularities of the integrands of f_1 and f_2 distort the integration contours, $u \leq 0$, until j reaches α_{c+} . This can be seen by noting that, for u real and t negative,

$$\begin{aligned} \text{Im} a = \text{Im} b = \text{Im} c = \text{Im} \beta^2 \\ = 2A(-t)^{1/2}(\xi + 1 - 2\alpha - \frac{1}{2}\gamma t - 2\gamma u). \end{aligned} \quad (3.4)$$

Since α_{c+} corresponds to $\xi = 2\alpha - 1 + \frac{1}{2}\gamma t$, these imaginary parts are all positive for j to the right of α_{c+} and $u \leq 0$. No singularity of the integrand migrates across the integration contour.

When j passes under α_{c+} , the singularities of the integrands of f_1 and f_2 are distributed as shown in Fig. 3. For a continuation above α_{c+} , the integration contour passes under u_{a-} and u_{c-} . Since u_{a-} has a finite negative imaginary part, the u contour must be slightly distorted when one passes above α_{c+} . The discontinuities of f_1 and f_2 are given by expressions similar to Eq. (3.2), except the limits are u_{c-} and u_{a-} . For j near α_{c+} , f_1 dominates, and f has a logarithmic singularity at $j = \alpha_{c+}$.

When we continue down to $j = \alpha_+$, or $\xi = 1 + \gamma t$, there is a possible singularity due to a pinch between u_{b-} and u_{c-} . Since u_{b-} approaches u_{c-} from above, this pinch develops only when one passes

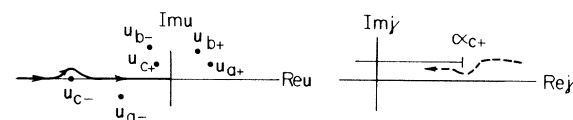


FIG. 3. Distribution of the singularities of integrands of f_1 and f_2 when j is continued under α_{c+} .

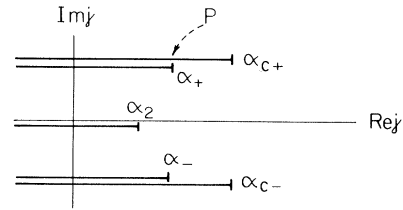


FIG. 4. Singularities of f for $t < 0$. α_+ is not a singular point when approached along path P . This is the approach relevant for the bootstrap of the Pomeron pole.

under α_{c+} . As j passes below α_{c+} down to α_+ , Eq. (3.4) shows that the imaginary parts of a , b , and c are nonzero except at u_{c-} , which slides along the negative u axis. Thus no deformation of the u contour occurs, and the discontinuities of f_1 and f_2 across branch lines drawn up to α_+ are given by expressions similar to Eq. (3.2) with limits u_{b-} and u_{c-} . Both f_1 and f_2 have the behavior near α_+

$$f_{1,2} \sim \text{const} + \text{const}' [j - \alpha_+(t)] \ln[j - \alpha_+(t)]. \quad (3.5)$$

The function f is a real analytic function of j , so it is singular at α_{c-} and α_- , with discontinuities at these singularities that are minus the complex conjugates of the discontinuities at α_{c+} and α_+ . The complete set of branch points of f for $t < 0$ is shown in Fig. 4.

There is no problem in continuing Eq. (2.2) to $t > 0$, because our discussion in Sec. I assures us that f is analytic at $t = 0$ for large positive j . The analysis we have just given can be repeated for $t > 0$, and is simplified because all possible singularities are real.

IV. BOOTSTRAPPING THE POMERANCHON

We have mentioned in the Introduction that when the Pomeron is a pole on a linear trajectory, and $\alpha'(0)$ is finite, the pole cannot have $\alpha(0) = 1$ unless certain couplings vanish. One way of stating the matter is that the two-Pomeron cut integral diverges for $j = \alpha(t)$ as $t \rightarrow 0$. However, the coefficient of the divergent term is proportional to $[\alpha'(0)]^{-1}$, so this unpleasant situation might be avoided if the Pomeron were a pair of poles on Schwarz trajectories. Similarly, in connection with single-particle inclusive cross sections the question of the vanishing of the triple-Pomeron vertex involves the assumption that $\alpha'(0)$ is finite.¹⁰ Here we shall show that choosing the Pomeron trajectory to be of the Schwarz type does not help, and one must have certain couplings vanish in appropriate limits,

as discussed in Ref. 7, in order to achieve $\alpha(0)=1$. Likewise, the triple-Pomeranchon coupling cannot be made finite by choosing a Pomeranchon trajectory of the Schwarz type.

When we set $j = \alpha_+(t)$ in $f(t, j)$, and $t < 0$, we must approach α_+ from above in Fig. 4. As stated in Sec. III, when α_+ is approached in this manner, u_{b-} and u_{c-} do not form a pinch, and f is regular. In Eq. (2.2) the factors $(u - u_{b-})$ and $(u - u_{c-})$ cancel between numerator and denominator in f_1 and f_2 . It is now easy to see that as $t \rightarrow 0$, f_1 diverges logarithmically at $u=0$ due to the motion of u_{a-} and u_{c+} up to $u=0$. Because only these two factors are involved, it is straightforward to calculate the leading behavior as $t \rightarrow 0$:

$$f(t, \alpha_+(t)) \sim -\frac{1}{\gamma} \ln(t+i\epsilon). \quad (4.1)$$

This result is half what one would obtain by first setting $A=0$ (the limit of a linear trajectory). Thus, the bootstrapping of Schwarz trajectories encounters the same difficulty as the bootstrapping of a linear trajectory.

APPENDIX A

Our first demonstration of the importance of the function $f(t, j)$ of Eq. (1.1) is based on the

$$V(s, t) = \frac{1}{16\pi^2 \Delta^{1/2}(s, m^2, m^2)} \int_{-\infty}^0 dt_1 \int_{-\infty}^0 dt_2 \frac{\theta(-\Delta(t, t_1, t_2) + t t_1 t_2 / k^2)}{[-\Delta(t, t_1, t_2) + t t_1 t_2 / k^2]^{1/2}} M(s, t_1) M^*(s, t_2), \quad (A2)$$

with $4sk^2 = \Delta(s, m^2, m^2)$, and $M(s, t)$ are the invariant amplitudes associated with the blobs. (See Fig. 6.) In principle, of course, even within the framework of this simple model, it is necessary to know the off-shell behavior of the scattering amplitudes.

Leaving aside for a moment the question of what $V(P, K, Q)$ is, we may simplify the integral equation for $A(P, K, Q)$ by making a "partial wave" diagonalization. We introduce a set of scalar variables

$$\begin{aligned} P^2 = u, \quad z = P \cdot Q / (ut)^{1/2}, \quad y = -\tilde{P} \cdot \tilde{K} / (\tilde{P}^2 \tilde{K}^2)^{1/2}, \\ K^2 = v, \quad \zeta = K \cdot Q / (vt)^{1/2}, \quad y_0 = -\tilde{P} \cdot \tilde{P}' / (\tilde{P}^2 \tilde{P}'^2)^{1/2}, \\ P'^2 = u', \quad z' = P' \cdot Q / (u't)^{1/2}, \quad y' = -\tilde{P}' \cdot \tilde{K}' / (\tilde{P}'^2 \tilde{K}'^2)^{1/2}, \end{aligned} \quad (A3)$$

where for any vector N , $\tilde{N} = N - Q(N \cdot Q)/Q^2$. The y 's in turn may be expressed in terms of the sub-energies $s = (P - K)^2$, $s_0 = (P - P')^2$, and $s' = (P' - K)^2$ as

$$\begin{aligned} y &= \frac{\cosh \Theta(u, v) - z\zeta}{[(1-z^2)(1-\zeta^2)]^{1/2}}, \\ y_0 &= \frac{\cosh \Theta_0(u, u') - zz'}{[(1-z^2)(1-z'^2)]^{1/2}}, \\ y' &= \frac{\cosh \Theta'(u', v) - z'\zeta}{[(1-z'^2)(1-\zeta^2)]^{1/2}}, \end{aligned} \quad (A4)$$

multiperipheral model. The equation for the absorptive part of the nonforward elastic amplitude, A , is

$$\begin{aligned} A(P, K, Q) = V(P, K, Q) \\ + \frac{2}{(2\pi)^4} \int d^4 P' V(P, P', Q) S(P', Q) A(P', K, Q), \end{aligned} \quad (A1)$$

which has the kinematic structure shown in Fig. 5. In terms of scalar variables we have $s = (P - K)^2$, $t = Q^2$, and on the mass shell $P \cdot Q = K \cdot Q = 0$, $P^2 + \frac{1}{4}Q^2 = K^2 + \frac{1}{4}Q^2 = M^2$ for equal-mass external particles. Here $V(P, K, Q)$ is the absorptive part of the basic blobs in the multiperipheral chain;

$$S(P', Q) = [m^2 - (P' - \frac{1}{2}Q)^2]^{-1} [m^2 - (P' + \frac{1}{2}Q)^2]^{-1},$$

with m the mass along the chain; our normalization is such that on shell, for $Q=0$ (forward scattering)

$$A(s, t=0) = \Delta^{1/2}(s, M^2, M^2) \sigma_{\text{total}}(s).$$

If the basic blobs themselves consist of two-particle scattering amplitudes, then on the mass shell V is given by elastic unitarity:

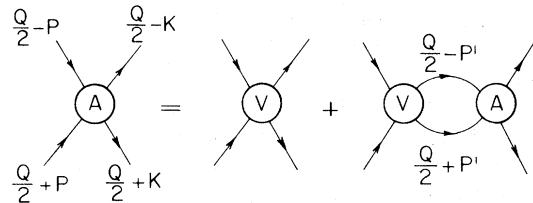
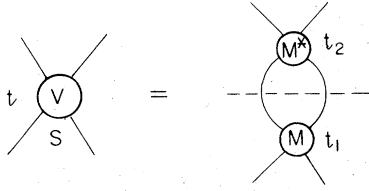


FIG. 5. Kinematic structure of the multiperipheral equation. The momentum labels on the external lines on the right-hand side are the same as on the left.

FIG. 6. Elastic unitarity for the "potential" V .

where

$$\begin{aligned} \cosh \Theta(u, v) &= \frac{s - u - v}{2(uv)^{1/2}}, \\ \cosh \Theta_0(u, u') &= \frac{s_0 - u - u'}{2(uv)^{1/2}}, \\ \cosh \Theta'(u', v) &= \frac{s' - u' - v}{2(u'v)^{1/2}}. \end{aligned} \quad (\text{A5})$$

For technical reasons we imagine $u, v < 0$, although ultimately on the mass shell they take on the positive values $u = v = M^2 - \frac{1}{4}t$. The appropriate transform is

$$A_j(u, z; v, \zeta; t) = V_j(u, z; v, \zeta; t)$$

$$+ \frac{1}{16\pi^4} \int_{-\infty}^0 du' \int_{-1}^1 \frac{dz'}{(1-z'^2)^{1/2}} V_j(u, z; u', z'; t) A_j(u', z'; v, \zeta; t) [(m^2 - u' - \frac{1}{4}t)^2 - u' t z'^2]^{-1}. \quad (\text{A9})$$

For our present illustrative purposes, we solve this in the first Fredholm approximation. We find

$$A_j(u, z; v, \zeta; t) = V_j(u, z; v, \zeta; t) + \frac{N_j(u, z; v, \zeta; t)}{D(t, j)}, \quad (\text{A10})$$

where

$$N_j(u, z; v, \zeta; t) = \frac{1}{16\pi^4} \int_{-\infty}^0 du' \int_{-1}^1 \frac{dz'}{(1-z'^2)^{1/2}} \frac{V_j(u, z; u', z'; t) V_j(u', z'; v, \zeta; t)}{(m^2 - u' - \frac{1}{4}t)^2 - u' t z'^2}, \quad (\text{A11})$$

$$D(t, j) = 1 - \frac{1}{16\pi^4} \int_{-\infty}^0 du \int_{-1}^1 \frac{dz}{(1-z^2)^{1/2}} \frac{V_j(u, z; u, z; t)}{(m^2 - u - \frac{1}{4}t)^2 - u t z^2}.$$

There are two sources of singularities in j : singularities that occur in the kernel V_j itself and those associated with the Fredholm denominator $D(t, j)$. For example, if $D(t, j) = 0$ for some $j = \alpha(t)$, this determines the Regge poles. As for V_j , note that it is given as an integral of the input $V(s, \dots)$ over an infinite range of s weighted with Q_j . Any finite part of the integration contributes an analytic function of j (except for trivial and irrelevant poles of Q_j at negative integers). The dynamical singularities arise from the high-energy tail of $V(s, \dots)$ for which we shall use our model given by elastic unitarity. In addition we

$$A_j(u, z; v, \zeta; t) = \int_{L^2} ds Q_j(y) A(s; u, z; v, \zeta; t), \quad (\text{A6})$$

where $ds = 2[uv(1-z^2)(1-\zeta^2)]^{1/2} dy$. Similarly

$$V_j(u, z; v, \zeta; t) = \int_{L^2} ds Q_j(y) V(s; u, z; v, \zeta; t), \quad (\text{A7})$$

$$V_j(u, z; u', z'; t) = \int_{L^2} ds_0 Q_j(y_0) V(s_0; u, z; u', z'; t).$$

In these equations L is the lowest mass occurring in V which would be $4m^2$ in our present model, and Q_j is a Legendre function of the second kind. The inversion formula to recover $A(s; \dots)$ given $A_j(\dots)$ is

$$A(s; \dots) = \int_{c-i\infty}^{c+i\infty} \frac{dj(2j+1)}{2\pi i} A_j(\dots) P_j(y) \times \frac{1}{2} [uv(1-z^2)(1-\zeta^2)]^{-1/2}. \quad (\text{A8})$$

Details about the partial-wave analysis are given in a paper by Abarbanel and Saunders.¹¹

The diagonalized equation is

shall assume that off-shell effects may be neglected and that the amplitudes $M(s, t)$ are adequately approximated by a single Regge pole:

$$M(s, t) = m(t) s^{\alpha(t)}. \quad (\text{A12})$$

For high-energy s we now have

$$V(s, t) = \frac{1}{16\pi^2 s} \int_{-\infty}^0 dt_1 \int_{-\infty}^0 dt_2 \frac{\theta(-\Delta(t, t_1, t_2))}{[-\Delta(t, t_1, t_2)]^{1/2}} \times m(t_1) m^*(t_2) s^{\alpha(t_1) + \alpha(t_2)}. \quad (\text{A13})$$

The singularities of V_j are correctly given by

$$V_j(u, z; v, \xi; t) = \int_{s^*}^{\infty} ds V(s, t) Q_j(y), \quad (A14)$$

where s^* is some large energy. When s is large

$$y \sim \frac{s}{2[uw(1-z^2)(1-\xi^2)]^{1/2}}, \quad (A15)$$

$$Q_j(y) \sim \frac{\pi^{1/2} \Gamma(j+1)}{\Gamma(j+\frac{3}{2})} [uw(1-z^2)(1-\xi^2)]^{(j+1)/2} s^{-j-1}.$$

Our model for V_j then turns out to be

$$V_j(u, z; v, \xi; t) = \frac{\Gamma(j+1)}{\Gamma(j+\frac{3}{2}) 16\pi^{3/2}} [uw(1-z^2)(1-\xi^2)]^{(j+1)/2}$$

$$\times \int_{-\infty}^0 dt_1 \int_{-\infty}^0 dt_2 \frac{\theta(-\Delta(t, t_1, t_2))}{[-\Delta(t, t_1, t_2)]^{1/2}} \frac{m(t_1)m^*(t_2) s^{*-j-1+\alpha(t_1)+\alpha(t_2)}}{j+1-\alpha(t_1)-\alpha(t_2)}. \quad (A16)$$

We see here the emergence of the integral $f(t, j)$ (for the case where the trajectories are the same) in the potential V_j , aside from the appearance of the factor

$$m(t_1)m^*(t_2) s^{*-j-1+\alpha(t_1)+\alpha(t_2)}$$

which serves to cut off the integral for large $-t_1, -t_2$; in our definition of $f(t, j)$ we simulated this by a square cutoff at $-t_0$ since only the region near $t_1, t_2 \approx 0$ is important in the singularity structure of the integral. Finally, we note that the Fredholm denominator $D(t, j)$ becomes

$$D(t, j) = 1 - \frac{I(t, j)}{\pi} \int_{-\infty}^0 dt_1 \int_{-\infty}^0 dt_2 \frac{\theta(-\Delta(t, t_1, t_2))}{[-\Delta(t, t_1, t_2)]^{1/2}} m(t_1)m^*(t_2) \frac{s^{*-j-1+\alpha(t_1)+\alpha(t_2)}}{j+1-\alpha(t_1)-\alpha(t_2)}, \quad (A17)$$

where

$$I(t, j) = \frac{\Gamma(j+1)}{256\pi^{9/2} \Gamma(j+\frac{3}{2})} \int_{-\infty}^0 du (-u)^{j+1} \int_{-\frac{1}{4}t}^1 \frac{dz (1-z^2)^{j+1/2}}{(m^2 - u - \frac{1}{4}t)^2 - utz^2}. \quad (A18)$$

The function $I(t, j)$ has singularities for $j > 0$, but these are spurious and a result of our omission of off-shell damping effects. If these are properly taken into account, $I(t, j)$ is seen to be real and positive for $j > -1$ and all $t < 0$. The coefficient of $I(t, j)$ in Eq. (A17) is our fundamental integral $f(t, j)$, aside from the modification of the cutoff mentioned above.

A much more detailed treatment of both the low- and high-energy parts of the potential, together with a discussion of off-shell effects and a more accurate solution of the integral equation, is presented by Abarbanel *et al.*¹⁰ and by Goldberger.⁹

APPENDIX B

A second demonstration of the relevance of $f(t, j)$ can be obtained by studying the t -channel partial-wave amplitude for Reggeon-Reggeon scattering. We deal with the amplitude $g(t_1, t_2; t, j; t'_1, t'_2)$, where the t_i, t'_i are Reggeon masses squared, and t and j are the t -channel energy and angular momentum, respectively. The structure of the amplitude is shown in Fig. 7. We take g and the Reggeons appearing in intermediate states to have even signature. According to the Reggeon calculus,¹² each intermediate state in Fig. 7 has a

nonrelativistic energy denominator

$$\frac{1}{(j-1) - (j_1-1) - (j_2-1)} \frac{\cos[\frac{1}{2}\pi(j_1+j_2)]}{\sin(\frac{1}{2}\pi j_1) \sin(\frac{1}{2}\pi j_2)}. \quad (B1)$$

In addition there is a propagator for each Reggeon, $[j_i - \alpha_i(-\vec{q}_i^2)]^{-1}$, where \vec{q}_i are two-dimensional vectors and the α_i the Regge trajectories. The product of energy denominators and propagators is then acted on by

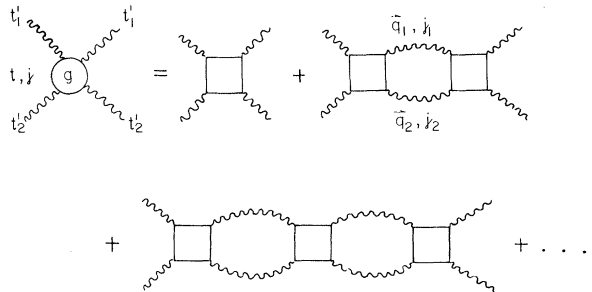


FIG. 7. Structure of the Reggeon-Reggeon scattering amplitude. The blocks are the sum of all two-Reggeon irreducible Gribov diagrams.

$$\int \frac{d^2 q_1}{(2\pi)^2} \int \frac{d^2 q_2}{(2\pi)^2} \int \frac{d j_1}{2\pi i} \int \frac{d j_2}{2\pi i} (2\pi)^2 \delta(\vec{q} - \vec{q}_1 - \vec{q}_2), \quad (\text{B2})$$

where the integrals over j_i go counterclockwise around the propagators. The over-all momentum is $t = -\vec{q}^2$. Note the elementary kinematical relation

$$\begin{aligned} \int d^2 q_1 \int d^2 q_2 \delta(\vec{q} - \vec{q}_1 - \vec{q}_2) &= \int_{-\infty}^0 dt_1 \int_{-\infty}^0 dt_2 \int d^2 q_1 \int d^2 q_2 \delta(\vec{q} - \vec{q}_1 - \vec{q}_2) \delta(\vec{q}_1^2 + t_1) \delta(\vec{q}_2^2 + t_2) \\ &= \int_{-\infty}^0 dt_1 \int_{-\infty}^0 dt_2 \frac{\theta(-\Delta(t, t_1, t_2))}{[-\Delta(t, t_1, t_2)]^{1/2}}. \end{aligned} \quad (\text{B3})$$

Using this, each two-Reggeon link in Fig. 7 contributes a factor

$$\int_{-\infty}^0 d\bar{t}_1 \int_{-\infty}^0 d\bar{t}_2 \frac{\theta(-\Delta(t, \bar{t}_1, \bar{t}_2))}{[-\Delta(t, \bar{t}_1, \bar{t}_2)]^{1/2}} \frac{\cos(\frac{1}{2}\pi [\alpha(\bar{t}_1) + \alpha(\bar{t}_2)])}{\sin[\frac{1}{2}\pi \alpha(\bar{t}_1)] \sin[\frac{1}{2}\pi \alpha(\bar{t}_2)]} \frac{1}{j+1 - \alpha(\bar{t}_1) - \alpha(\bar{t}_2)}. \quad (\text{B4})$$

The discontinuity of g across the two-Reggeon cut is now easily found to be

$$\begin{aligned} \frac{1}{2i} [g(t_1, t_2; t, j+i\epsilon; t'_1, t'_2) - g(t_1, t_2; t, j-i\epsilon; t'_1, t'_2)] \\ = \pi \sin(\frac{1}{2}\pi j) \int_{-\infty}^0 d\bar{t}_1 \int_{-\infty}^0 d\bar{t}_2 \frac{\theta(-\Delta(t, \bar{t}_1, \bar{t}_2))}{[-\Delta(t, \bar{t}_1, \bar{t}_2)]^{1/2}} \frac{\delta(j+1 - \alpha(\bar{t}_1) - \alpha(\bar{t}_2))}{\sin[\frac{1}{2}\pi \alpha(\bar{t}_1)] \sin[\frac{1}{2}\pi \alpha(\bar{t}_2)]} \\ \times g(t_1, t_2; t, j; \bar{t}_1, \bar{t}_2) g(\bar{t}_1, \bar{t}_2; t, j-i\epsilon; t'_1, t'_2). \end{aligned} \quad (\text{B5})$$

At the threshold of the two-Reggeon cut, the δ function requires $\bar{t}_i = \frac{1}{4}t$. If we set all $t_i, \bar{t}_i, t'_i = \frac{1}{4}t$ and ignore further dependence on the Reggeon masses, we can remove the g 's from the integral and we have a simple mapping problem of the form

$$\frac{1}{2i} [g^{-1}(t, j+i\epsilon) - g^{-1}(t, j-i\epsilon)] = -\rho(t, j). \quad (\text{B6})$$

The solution is

$$g^{-1}(t, j) = R(t, j) + \sin(\frac{1}{2}\pi j) \int_{-\infty}^0 dt_1 \int_{-\infty}^0 dt_2 \frac{\theta(-\Delta(t, t_1, t_2))}{[-\Delta(t, t_1, t_2)]^{1/2}} \frac{1}{\sin[\frac{1}{2}\pi \alpha(t_1)] \sin[\frac{1}{2}\pi \alpha(t_2)] [j+1 - \alpha(t_1) - \alpha(t_2)]}, \quad (\text{B7})$$

where $R(t, j)$ does not share the branch points of the integral. Finally, the contribution of the two-Reggeon cut to the physical partial-wave amplitude is proportional to $g(t, j)$,¹³ with the proportionality factor analytic at the branch points of $g(t, j)$.

There are two features to be noted in Eq. (B7). The cut is multiplied by $\sin(\frac{1}{2}\pi j)$, so it disappears at even-signature integers. This behavior is of

course required, but it does not occur in the multiperipheral model. The second point is that the sign of the cut term is opposite to that found in the multiperipheral model. In any case, both models lead to what is essentially the cut integral introduced in Eq. (1.1). [The singularities associated with the signature factors in Eq. (B7) are spurious.]

*Research supported in part by the National Science Foundation under Grants No. GP-36740X and GP-16147A1.

¹We use the standard notation: The square of the total energy in the (s) scattering channel is s and the (negative) square of the momentum transfer is t ; j is the angular momentum projection label appropriate to the t channel.

²J. H. Schwarz, Phys. Rev. **167**, 1342 (1967).

³H. Cheng and T. T. Wu, Phys. Rev. Lett. **24**, 1456

(1970); S.-J. Chang and T.-M. Yan, *ibid.* **25**, 1586 (1970).

⁴A. A. Anselm, G. S. Danilov, I. T. Dyatlov, and E. M. Levin, Yad. Fiz. **11**, 896 (1970) [Sov. J. Nucl. Phys. **11**, 500 (1970)]; J. Arafine and H. Sugawara, Phys. Rev. Lett. **25**, 1516 (1970); V. N. Gribov, I. Yu. Kobsarev, V. D. Mur, L. B. Okun, and V. S. Popov, Phys. Lett. **32B**, 129 (1970); J. Finkelstein, Phys. Rev. Lett. **24**, 172 (1970); R. Oehme, Phys. Rev. D **3**, 3217 (1971); **4**, 1485 (1971).

⁵R. Oehme, Phys. Rev. D 4, 1485 (1971).

⁶J. Finkelstein and F. Zachariasen, Phys. Lett. 34B, 631 (1971); J. R. Fulco and R. L. Sugar, Phys. Rev. D 4, 1919 (1971).

⁷J. B. Bronzan and C. G. Hui, Phys. Rev. D 5, 964 (1972).

⁸There are circumstances when this is not the rightmost singularity. See C.-I Tan and J.-M. Wang, Phys. Rev. Lett. 22, 1152 (1969).

⁹M. L. Goldberger, in Enrico Fermi School Varenna

Lectures, 1971 (to be published).

¹⁰H. Abarbanel, G. Chew, M. Goldberger, and L. Saunders, Ann. Phys. (N.Y.) 73, 156 (1972).

¹¹H. Abarbanel and L. Saunders, Phys. Rev. D 2, 711 (1970).

¹²V. N. Gribov, Zh. Eksp. Teor. Fiz. 53, 654 (1967) [Sov. Phys.-JETP 26, 414 (1968)].

¹³V. N. Gribov, I. Ya. Pomeranchuk, and K. A. Ter-Martirosyan, Phys. Rev. 139, B184 (1965).

PHYSICAL REVIEW D

VOLUME 8, NUMBER 10

15 NOVEMBER 1973

Scale Dimension of the Chiral-Symmetry-Breaking Hamiltonian

Fayyazuddin*

Rutherford High Energy Laboratory, Chilton, Didcot, Berkshire, England

Riazuddin

Institute of Physics, University of Islamabad, Islamabad, Pakistan

(Received 14 June 1973)

We present arguments based on positivity conditions and light-cone analysis for the structure functions W_4 and W_5 (which occur in neutrino scattering) to conclude that if they scale as $\nu^p W_{4,5}(\nu, q^2) \rightarrow F_{4,5}(\xi)$, then $p = 2$. We also get the following bound on the scale dimension l_u of the chiral-symmetry-breaking Hamiltonian: $-\frac{5}{2} \geq l_u > -4$. Further, if we assume that fractional dimensions are not admissible, we get $l_u = -3$.

I. INTRODUCTION

The scaling observed in the SLAC electron scattering experiments has generated considerable interest in light-cone analysis of structure functions for inelastic electron and neutrino scattering on nucleons. This is due to the fact that in the scaling limit, one is probing the structure of the current commutator near the light cone. The structure functions are related to the Fourier transform of the current commutator. The scaling behavior of the structure functions W_1 , W_2 , and W_3 which are connected with conserved currents is now more or less established both theoretically and experimentally. It is natural to assume that the other two structure functions W_4 and W_5 which occur in neutrino scattering due to nonconservation of the axial-vector current also scale. Their scaling behavior has important bearing on the nature of the chiral symmetry breaking. In particular if W_4 and W_5 scale ($\nu \rightarrow \infty$, $\xi = q^2/2m\nu$ fixed) as

$$\nu^p W_{4,5}(\nu, q^2) \rightarrow F_{4,5}(\xi),$$

it is important to know p . This is because p can be related to the scale dimension l_u of the chiral-symmetry-breaking Hamiltonian.¹⁻⁵ Moreover, the value of p is important in deriving sum rules^{4,6}

which W_4 and W_5 satisfy in the scaling limit.

The purpose of this paper is to present arguments based on light-cone analysis and positivity conditions⁷ for the structure functions $W_{4,5}$ which lead to the results (a) $l_u \leq -\frac{5}{2}$ (this result implies $l_u = -3$ if only integers are allowed), (b) $p = 2$, (c) if $D(\nu, q^2) \equiv q^4 [W_4 - (2m\nu/q^2)W_5]$ scales as $\nu^{-p_1} \phi(\xi)$, then $p_1 = 0$.

For the derivation of result (a), we do not require positivity conditions but we need two assumptions: (1) the equal-time commutator $[\partial_\mu J_\mu(\vec{z}, 0), \partial_\nu \bar{J}_\nu(0)]$ is nonzero and (2) the scalar operator ω which occurs in the light-cone expansion of $D(p \cdot z, z^2)$ has scale dimension $l_\omega \leq -1$.

For the derivation of results (b) and (c), we make use of positivity conditions and three more assumptions: (3) $F_L(\xi) = 0$, where $F_L(\xi)$ is the scaling part of W_L (defined below), (4) the non-scaling part of W_L falls like $1/\nu$ and not like $1/\nu^\epsilon$, with $0 < \epsilon < 1$; (5) W_4 has the same scaling behavior as W_5 . The assumption (3) is the Callan and Gross⁸ sum rule and is generally believed to be true.

The plan of this paper is as follows. In Sec. II, we discuss the consequences of positivity conditions for $W_{4,5}$. In Sec. III, light-cone analysis for the function D is done. In Sec. IV we derive our main results.